


Type 2 diabetes influences intraepithelial corneal nerve parameters and corneal stromal-epithelial nerve penetration sites

Joshua Machet¹ , Mijeong Park¹, Alexander Richardson¹, Michael Carnell², Margaret A Mouat¹, Nicola J Smith¹, Nigel Turner^{1,3}, Blake J Cochran¹, Kerry-Anne Rye¹, Nick Di Girolamo^{1*}

¹School of Biomedical Sciences, Faculty of Medicine and Health, University of New South Wales, Sydney, NSW, Australia, ²Katharina Gaus Light Microscopy Facility, Mark Wainwright Analytical Centre, University of New South Wales, Sydney, NSW, Australia, and ³Victor Chang Cardiac Research Institute, Sydney, NSW, Australia

Keywords

Corneal stromal-epithelial nerve penetration sites, Diabetic peripheral neuropathy, Intraepithelial corneal basal nerves

*Correspondence

Nick Di Girolamo
Tel: +61-419221556
E-mail address:
n.digirolamo@unsw.edu.au

J Diabetes Investig 2023; 14: 591–601

doi: [10.1111/jdi.13974](https://doi.org/10.1111/jdi.13974)

ABSTRACT

Introduction: The quantification of intraepithelial corneal basal nerve parameters by *in vivo* confocal microscopy represents a promising modality to identify the earliest manifestations of diabetic peripheral neuropathy. However, its diagnostic accuracy is hampered by its dependence on neuron length, with minimal consideration for other parameters, including the origin of these nerves, the corneal stromal-epithelial nerve penetration sites. This study sought to utilize high-resolution images of murine corneal nerves to analyze comprehensively the morphological changes associated with type 2 diabetes progression.

Materials and Methods: β III-Tubulin immunostained corneas from prediabetic and type 2 diabetic mice and their respective controls were imaged by scanning confocal microscopy and analyzed automatically for nerve parameters. Additionally, the number and distribution of penetration sites was manually ascertained and the average length of the axons exiting them was computed.

Results: The earliest detectable changes included a significant increase in nerve density ($6.06 \pm 0.41\%$ vs $8.98 \pm 1.99\%$, $P = 0.03$) and branching ($2867.8 \pm 271.3/\text{mm}^2$ vs $4912.1 \pm 1475.3/\text{mm}^2$, $P = 0.03$), and in the number of penetration sites (258.80 ± 20.87 vs 422.60 ± 63.76 , $P = 0.0002$) at 8 weeks of age. At 16 weeks, corneal innervation decreased, most notably in the periphery. The number of penetration sites remained significantly elevated relative to controls throughout the monitoring period. Similarly, prediabetic mice exhibited an increased number of penetration sites (242.2 ± 13.55 vs 305.6 ± 30.96 , $P = 0.003$) without significant changes to the nerves.

Conclusions: Our data suggest that diabetic peripheral neuropathy may be preceded by a phase of neuron growth rather than regression, and that the peripheral cornea is more sensitive than the center for detecting changes in innervation.

INTRODUCTION

Diabetes is a leading public health concern causing significant and increasing morbidity and mortality. A substantial component of this is attributable to the complications of diabetes, which include diabetic peripheral neuropathy (DPN). DPN affects up to 51% of diabetic adults over their lifetime and increases their risk of developing neuropathic ulcers and requiring lower limb

amputations¹. Investigations that can diagnose and monitor advanced DPN are well established, however, methods for identifying the earliest subclinical stages, where interventions would have the most impact, remain elusive². As part of the peripheral nervous system, corneal nerves are affected in DPN and therefore represent a promising surrogate structural biomarker for detecting and monitoring its development³.

The presence of hyper-reflective nerve fibers within the external and transparent cornea conveniently enables their

Received 21 November 2022; revised 16 December 2022; accepted 1 January 2023

visualization with minimally invasive *in vivo* confocal microscopy (IVCM)⁴. Since the pioneering study by Ahmed *et al.*⁵, where they achieved a diagnostic accuracy of 85% sensitivity and 84% specificity, most investigations have failed to reach or significantly improve upon their results⁶. Previous studies have predominantly relied on corneal nerve fiber length to discriminate between healthy subjects and patients with diabetes⁶. However, the lack of improvement indicates an inherent diagnostic limitation of this metric. Additionally, nerve length is reduced in a plethora of other peripheral neuropathies and neurodegenerative conditions⁷. Accordingly, when used as a screening tool, the lack of specificity associated with nerve fiber length could be problematic in distinguishing between different etiologies.

A promising approach to overcoming these shortcomings is to identify new corneal nerve parameters. Mouse models represent an excellent avenue to pursue this ambition, since high-resolution immunostained images of neurons from the entire cornea of euthanized mice can be acquired using *ex vivo* scanning confocal microscopy. This technique allows for up to five times more nerve fibers to be captured compared with IVCM⁸, rendering it ideal for comprehensive morphological analysis of the intra-epithelial corneal basal nerves (ICBN). Combined with our murine-specific analytical modality, called noise-based segmentation (NoBS)⁹, both traditional and new neuronal features can be measured. To this end, we hypothesized that longitudinal analyzes of *db/db* mice, which represent a severe form of type 2 diabetes, as well as a cohort of mice fed a high-fat diet (HFD), representing an insulin-resistant prediabetic state, would facilitate a thorough characterization of ICBN changes seen in the progression of type 2 diabetes. In addition to previously used parameters, we included three new neural measurements to quantify ICBNs, including corneal stromal-epithelial nerve penetration sites (CSENPS) density, average fiber length/CSENPS, and axonal alignment. Analysis of these variables unexpectedly revealed an initial phase of neuron expansion during the early stages of type 2 diabetes before their anticipated degeneration. This phase may be important in identifying the earliest manifestations of DPN, and in conjunction with new parameters, could increase the sensitivity and specificity of IVCM. If translated to humans, these findings could facilitate earlier diagnosis of DPN and thus assist in reducing disease associated morbidity and mortality.

MATERIALS AND METHODS

Animals used and study design

Two animal models were used to identify and characterize the morphological changes in ICBNs associated with progressing type 2 diabetes. Notably, to reduce the number of animals used in experiments, all corneas were acquired *via* tissue sharing arrangements.

Model 1: Homozygous B6/BKS(D)-Lepr^{db}/J (*db/db*) ($n = 18$) and littermate homozygous wild-type control (+/+) ($n = 17$) mice were obtained from The Jackson Laboratory (Bar

Harbor, ME, USA) and were provided with standard chow (Specialty Feeds, Glen Forrest, WA, Australia) and water *ad libitum*. At 8, 16, and 32 weeks ($n \geq 5$ /group/time point), random blood glucose was measured using a glucometer (Accu-chek Performa II; Roche, Basel, Switzerland), mice were deeply anesthetized, euthanized by cervical dislocation and their eyes enucleated.

Model 2: Wild-type (C57BL/6J background) from Gpr371^{tm1d(EUCOMM)Wtsi}/Gpr371⁺ parents (MGI: 6150820) mice ($n = 12$), as used by Mouat *et al.*¹⁰, were fed a standard chow diet with 16% fat (Specialty Feeds) for 9 weeks. At 9 weeks of age, they were randomly divided into two groups; a HFD group ($n = 5$) and a control group ($n = 7$), which continued to receive standard chow. The HFD was formulated in-house based on rodent diet no. D12451 (Research Diets Inc., New Brunswick, NJ, USA) and contained 49% fat (Table S1). After 12 weeks (i.e., at 21 weeks of age), fasting blood glucose levels were measured using a blood glucometer, then mice were anesthetized, euthanized by cervical dislocation and their eyes enucleated.

Immunofluorescence

In brief, to identify ICBNs, resected corneas were incubated with 4 $\mu\text{g/mL}$ of primary polyclonal rabbit anti-mouse β III-tubulin antibody (Clone No. T2200; Sigma-Aldrich, St. Louis, MO, USA), then 10 $\mu\text{g/mL}$ of goat anti-rabbit Alexafluor⁵⁶⁸-conjugated secondary antibody (Invitrogen, Carlsbad, CA, USA). They were counterstained with 10 $\mu\text{g/mL}$ Hoechst 33342 (ThermoFisher Scientific, Waltham, MA, USA). Full details are provided in Appendix S1.

Image acquisition

One eye from each animal was imaged on a scanning confocal microscope (LSM 780 or LSM 880; Carl Zeiss, Oberkochen, Germany) using a 20 \times (0.8 numerical aperture) air objective lens. The signal arising from the Alexafluor⁵⁶⁸-conjugated secondary antibody was captured with a 561 nm laser and 570–610 nm emission filter, while the Hoechst 33342 nuclei counterstain was acquired with a 405 nm laser and 430–470 nm emission filter. For each cornea, two 425 \times 425 μm Z-stacks extending from the endothelium through to the superficial epithelium were taken. One encompassing the ICBNs that form the whorl and another of the peripheral fibers, $\sim 200 \mu\text{m}$ from the limbus in the first quadrant (Figure S1a,b,d). Finally, a multi-slice tile scan encompassing the entire cornea, from the mid-stroma through to the superficial epithelium was taken. From this, three 425 \times 425 μm Z-stacks from the remaining three quadrants were extracted in Zen black (Carl Zeiss).

Image analysis

A maximum intensity projection of the β III-tubulin channel was generated from each Z-stack of the slices containing ICBNs (i.e., excluding axons within the stroma and superficial intra-

epithelial corneal nerve terminals (ICNT; Figure S2) in ImageJ (National Institute of Health, Bethesda, MD, USA). Images of the whorl and peripheral ICBNs were quantified *via* our in-house developed ImageJ plugin, NoBS⁹ to determine their total length, density, number of branch points, and alignment. Length comprises the sum of all ICBNs present in the image (mm/mm^2). Density is a measure of nerve occupancy, expressed as a percentage and represents the proportion of pixels in the image that belong to ICBNs. Branch points include any region where two or more nerves meet ($\text{number}/\text{mm}^2$). Alignment was measured by comparing the angle of orientation of each ICBN pixel to all others in the image. The more similar they were to each other, the higher the score, on a unitless scale of 0–1 for each image⁹.

Analysis of corneal stromal-epithelial nerve penetration sites

Corneal stromal-epithelial nerve penetration sites (CSENPS) were manually identified by one of the authors (J.M.) using the same method as described previously⁹ with a minor modification. Instead of using a maximum intensity projection, each slice of the β III-tubulin-stained whole flat-mounted cornea was individually analyzed to prevent superficial structures from obstructing the CSENPS (Figure S2). The total number of CSENPS in each cornea was recorded, as were their locations (central or peripheral) (Figure S1a,b). To determine the average length of ICBNs exiting from the CSENPS, the length ($\text{length}/\text{mm}^2$) was divided by the number of CSENPS ($\text{CSENPS}/\text{mm}^2$), yielding the length/CSENPS. This calculation was performed independently in both the center and periphery. Additional details of CSENPS identification are provided in Appendix S1.

Statistical analysis

Statistical analysis was performed using Prism v9.0.2 software (GraphPad, La Jolla, CA, USA). A two-way ANOVA with Tukey's correction for multiple comparisons was used to compare nerve parameters, blood glucose, and the number of CSENPS between *db/db* and *+/+* mice. The distribution of CSENPS was compared using a two-way ANOVA with Tukey's correction for each time point separately. To compare mice fed a standard diet and those fed a HFD, unpaired *t*-tests were used to evaluate nerve parameters, blood glucose, and the number of CSENPS. A two-way ANOVA with Tukey's correction for multiple comparisons was used to compare the CSENPS distribution. Data were reported as mean \pm SD and regarded statistically significant when $P < 0.05$.

RESULTS

Intraepithelial corneal nerve fiber growth and regression in type 2 diabetes

The *db/db* mouse represents a severe model of type 2 diabetes, with profound hyperglycemia (Figure S3a) and is used widely in preclinical research for its accurate recapitulation of the metabolic events that define the human form of this disease¹¹. Accordingly, this model was employed to evaluate and quantify

changes undergone by ICBNs in aging *db/db* mice compared with *+/+* in order to magnify any subtle changes. In 8-week-old *db/db* mice, a strikingly visible increase in innervation was observed relative to controls. This phenomenon was more pronounced in the periphery (Figure 1a,g) but was also evident at the central whorl (Figure 1d,j). At 16 weeks of age, the effect subsided with no prominent visual change between the *db/db* mice and controls in terms of total nerve length, density, branching, or alignment (Figure 1b,e,h,k). Similarly, 32-week-old *db/db* mice demonstrated no significant aberrations in ICBN features relative to their control counterparts (Figure 1c,f,i,l).

Next, NoBS was applied to quantify these observations. At 8 weeks of age, a moderate increase in nerve fiber length and a statistically significant increase of 48% in density ($6.06 \pm 0.41\%$ vs $8.98 \pm 1.99\%$, $P = 0.03$) and 71% in branch points ($2867.8 \pm 271.3/\text{mm}^2$ vs $4912.1 \pm 1475.3/\text{mm}^2$, $P = 0.03$) was computed in the periphery (Figure 1m–o), with no significant increase observed at the whorl (Figure 1q–s). At 16 weeks, the initial increase in nerve parameters dissipated, with no significant changes in ICBN length, density, or branching in *db/db* mice compared with controls in the periphery or at the whorl. Likewise, no significant differences were found between the *db/db* mice and controls across all three ICBN parameters in 32-week-old mice. To further characterize the ICBNs, the local alignment of the same nerves was determined. No significant change in this feature was observed at either the whorl or periphery at all time points analyzed (Figure 1p,t).

Type 2 diabetes triggers an increase in the number of CSENPS and dynamic changes to ICBNs exiting these sites

Previous reports claim that the peripheral cornea harbors more CSENPS than the central region^{12,13}. This disproportionate distribution could explain why changes in nerve growth and degeneration are more substantial in the periphery. To investigate this hypothesis, the number, morphology, and distribution of CSENPS was ascertained. The total number of CSENPS significantly increased in *db/db* mice relative to controls at 8 (258.80 ± 20.87 vs 422.60 ± 63.76 , $P = 0.0002$), 16 (263.83 ± 38.31 vs 435.67 ± 81.91 , $P < 0.0001$), and 32 weeks (298.33 ± 38.31 vs 430.00 ± 40.42 , $P = 0.001$) by 63%, 65%, and 44%, respectively (Figure 2a). Evaluation of the geographical distribution of CSENPS revealed no difference in their density in the periphery compared with the center at each time point, within each group (Figure 2b).

The ICBNs emerging from CSENPS in the *db/db* mice at 8 weeks were morphologically similar to those from age-matched *+/+* animals at both the whorl and in the periphery (Figure 1). Analysis of the ICBN length exiting each CSENPS supports this observation, with no change identified between the two groups (Figure 2c,d). At 16 weeks, *db/db* mice exhibited severely truncated ICBNs, most notably in the periphery, resulting in a significant 47% decrease in ICBN length exiting the CSENPS relative to *+/+* mice (2.19 ± 0.77 mm vs

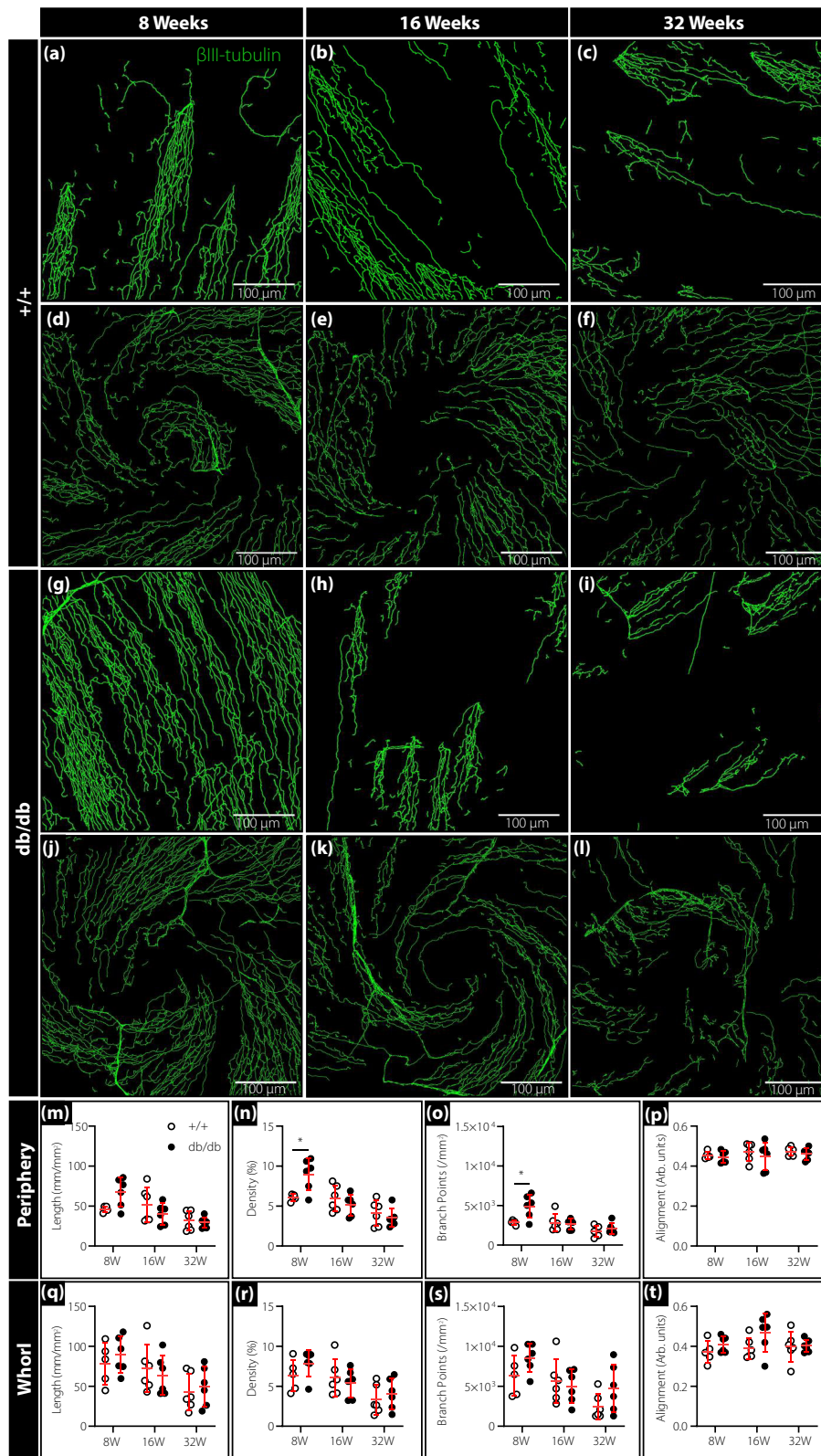


Figure 1 | Intraepithelial corneal innervation in mice with type 2 diabetes. Corneas from 8-, 16-, and 32-week-old +/+ control (a–f) and *db/db* (g–l) mice ($n = 5–6$ /group) were resected from euthanized mice and immunostained with β III-tubulin. After imaging, they were analyzed by NoBS (green trace) for various nerve parameters within the peripheral cornea (a–c and g–i) and at the whorl (d–f and j–l). Nerve fiber measurements included length (m and q), density (n and r), branch points (o and s), and alignment (p and t). White (+/+ control) and black (*db/db*) circles represent individual mice. Overlying red lines and plungers represent mean \pm SD (Scale bar = 100 μ m); * $P < 0.05$.

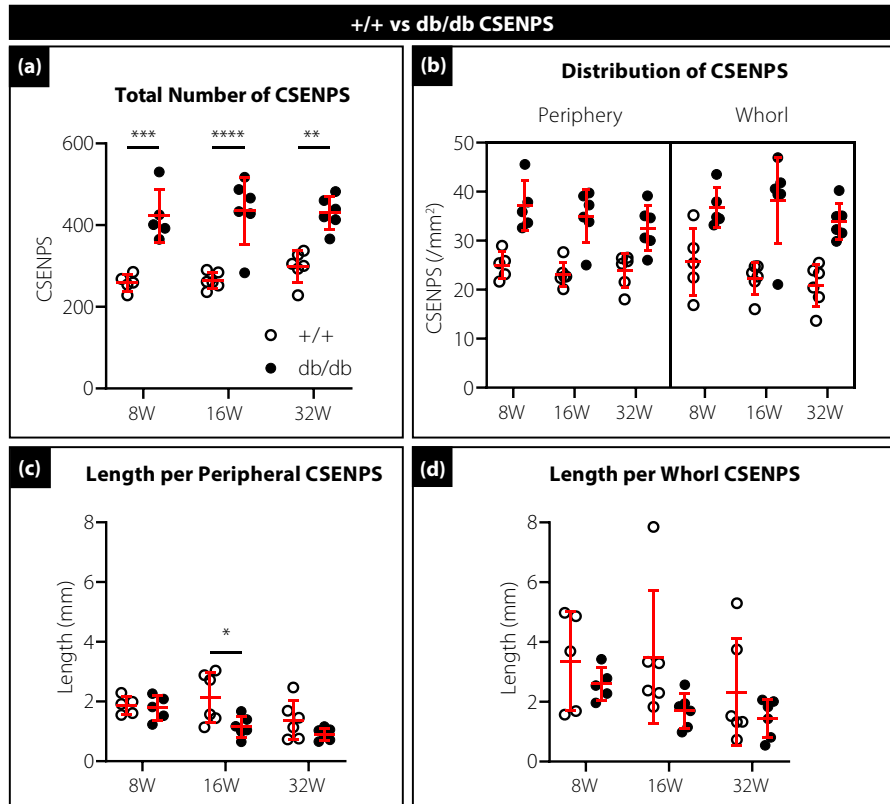


Figure 2 | Corneal stromal-epithelial nerve penetration sites in mice with type 2 diabetes. The total number of CSENPS in 8-, 16-, and 32-week-old +/+ control and *db/db* mice ($n = 5-6/\text{group}$) was counted (a) and their geographical distribution plotted and analyzed (b). The ICBN length exiting each CSENPS was calculated for fibers in the periphery (c) and at the center including the whorl (d). White (+/+ control) and black (*db/db*) circles represent individual mice. Overlying red lines and plungers represent mean \pm SD. * $P < 0.05$, ** $P < 0.01$, *** $P < 0.001$, **** $P < 0.0001$.

1.15 ± 0.35 mm, $P = 0.01$). At 32 weeks of age, CSENPS from both groups exhibited truncated ICBNs with no differences computed between the groups in either location.

Prediabetes minimally impacts intraepithelial corneal basal nerves

Mice fed a high-fat diet develop mild hyperglycemia (Figure S3b), hyperlipidemia, hyperinsulinemia, obesity, and impaired glucose tolerance, making them an ideal model to study prediabetes¹⁴. Previous studies¹⁵⁻¹⁷ demonstrated reduced corneal nerve density in these mice. However, there is a paucity of data on how other parameters are impacted. Accordingly, mice fed a HFD for 12 weeks were selected to investigate comprehensively the impact of prediabetes on the ICBNs. These mice appeared to have reduced ICBNs relative to those on a normal chow diet (Figure 3a-d), however, upon quantifying these observations, axon length, density, and branching in the periphery (Figure 3e-g) and at the whorl (Figure 3i-k) were not statistically different to chow-fed controls, despite a decreasing trend. Measurements of local ICBN alignment demonstrated a 22% increase in the periphery (0.39 ± 0.05 vs

0.48 ± 0.06 , $p = 0.01$; Figure 3h), that was not observed at the whorl (Figure 3l).

Prediabetes increases the number of CSENPS without impacting exiting ICBN fibers

As in the diabetic cohort, the number, morphology, and distribution of CSENPS were determined in the HFD-fed mice. The total number of CSENPS in the HFD group was 26% greater than in the control group (242.2 ± 13.55 vs 305.6 ± 30.96 , $P = 0.003$) (Figure 4a) and equally distributed between the center and periphery within groups (Figure 4b). The ICBNs exiting the CSENPS of mice fed a HFD appeared shorter and less numerous (Figure 3a-d). However, in both the center and periphery this reduction did not reach statistical significance (Figure 4c,d).

DISCUSSION

Herein, a novel, fully automatic, segmentation, and quantification modality was employed to analyze longitudinally high-resolution scanning confocal microscopy images of β III-tubulin immunostained corneal nerves from *db/db* and HFD-fed mice.

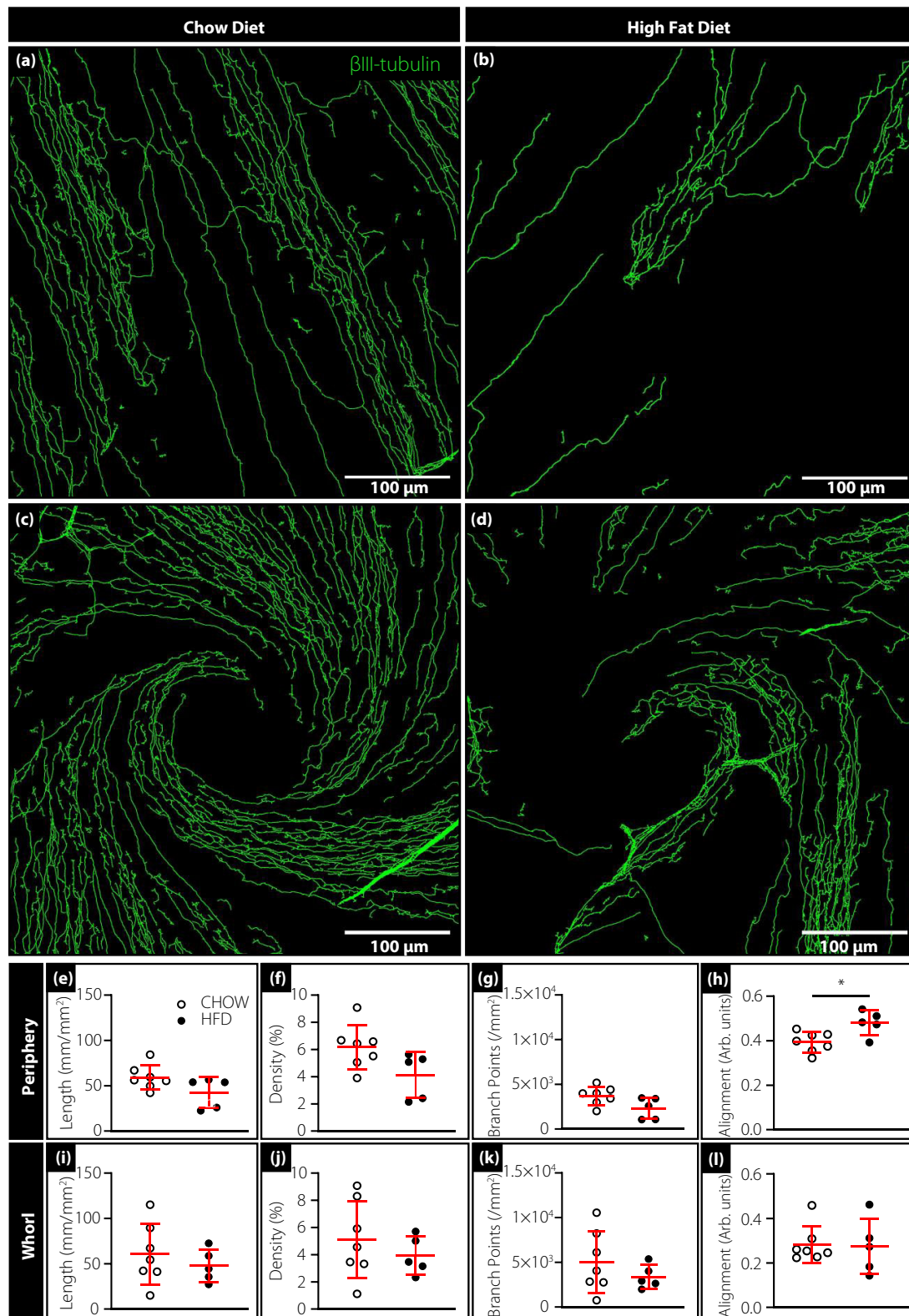


Figure 3 | Intraepithelial corneal innervation in prediabetic mice. Corneas from mice fed standard chow (a and c) or a HFD (b and d) ($n = 5$ – 7 /group) were resected from euthanized mice and immunostained for β III-tubulin. After imaging, they were analyzed by NoBS (green trace) for various nerve parameters within the peripheral cornea (a and b) and at the whorl (c and d). Nerve fiber measurements included length (e and i), density (f and j), branch points (g and k), and alignment (h and l). White (CHOW) and black (HFD) circles represent individual mice. Overlying red lines and plungers represent mean \pm SD (Scale bar = 100 μ m); * $P < 0.05$.

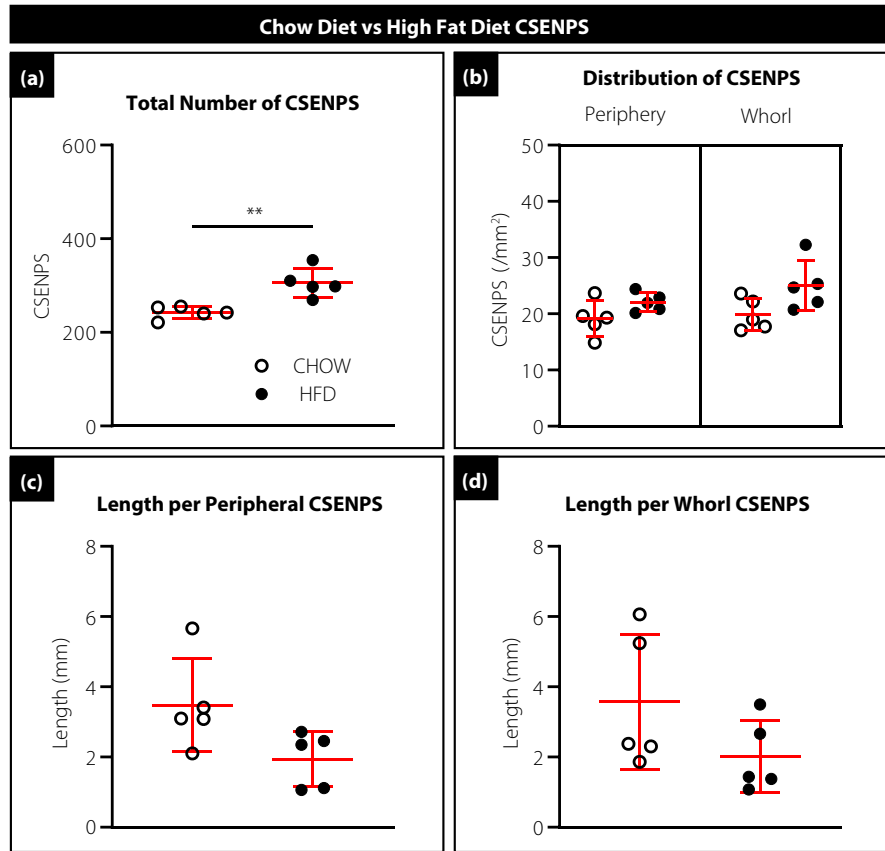


Figure 4 | Analysis of corneal stromal-epithelial nerve penetration sites in prediabetic mice. The total number of CSENPS in mice fed standard chow or a HFD ($n = 5\text{--}7/\text{group}$) was counted (a) and their geographical distribution ascertained and analyzed (b). The ICBN length exiting each CSENPS was calculated for fibers within the periphery (c) and at the center including the whorl (d). White (CHOW) and black (HFD) circles represent individual mice. Overlying red lines and plunger symbols represent mean \pm SD. $**P < 0.01$.

This study also produced an in-depth manual assessment of the number and location of CSENPS and the ICBNs exiting these structures. As a result, we identified an expansive phase of ICBN growth accompanied by an increasing number of CSENPS. Furthermore, this investigation provides the first information about how three new variables, including the number of CSENPS, fiber length/CSENPS, and axon alignment, are impacted by type 2 diabetes.

Previous studies in type 2 diabetic humans¹⁸ and animals^{19,20} have reported a reduction in corneal innervation when measured using IVCN. However, contrary to expectations, when evaluated with our highly sensitive platform, *db/db* mice exhibited increased corneal innervation at 8 weeks of age, most notably in the periphery. Accompanying this increase in density and branching (Figure 1), a profound increase in the number of CSENPS was also identified, which were evenly distributed between the central and peripheral regions (Figure 2a,b). Upon evaluating the length of ICBNs exiting each CSENPS, no difference between controls and diabetic animals was observed at 8 weeks of age (Figure 2c,d), indicating that the increased

innervation in *db/db* mice was primarily due to a rise in the number of CSENPS. This implies that during the early stages of type 2 diabetes, the stromal nerves are prompted to pierce the basement membrane, thereby increasing the density of these penetration sites, without directly impacting the ICBNs (Figure 5a). This hypothesis is supported by findings from the HFD-fed mice, which exhibited an increase in the number of CSENPS, with no change in ICBN parameters before the onset of type 2 diabetes (Figures 3 and 4).

The neurotrophic effect of insulin is well established²¹. In both humans²² and mice²³, systemic administration of insulin can ameliorate the deleterious effects of type 2 diabetes on the corneal nerves, either *via* protective or regenerative mechanisms. During the initial compensatory phase of type 2 diabetes, where insulin reaches supraphysiological levels to maintain glycemic control^{24,25}, its neurotrophic properties could explain the initial increase in ICBN parameters and density of CSENPS in the early stages of DPN (Figures 1 and 2). Lending further credence to this hypothesis is the substantially larger increase in CSENPS seen in *db/db* mice (57%) relative to HFD-

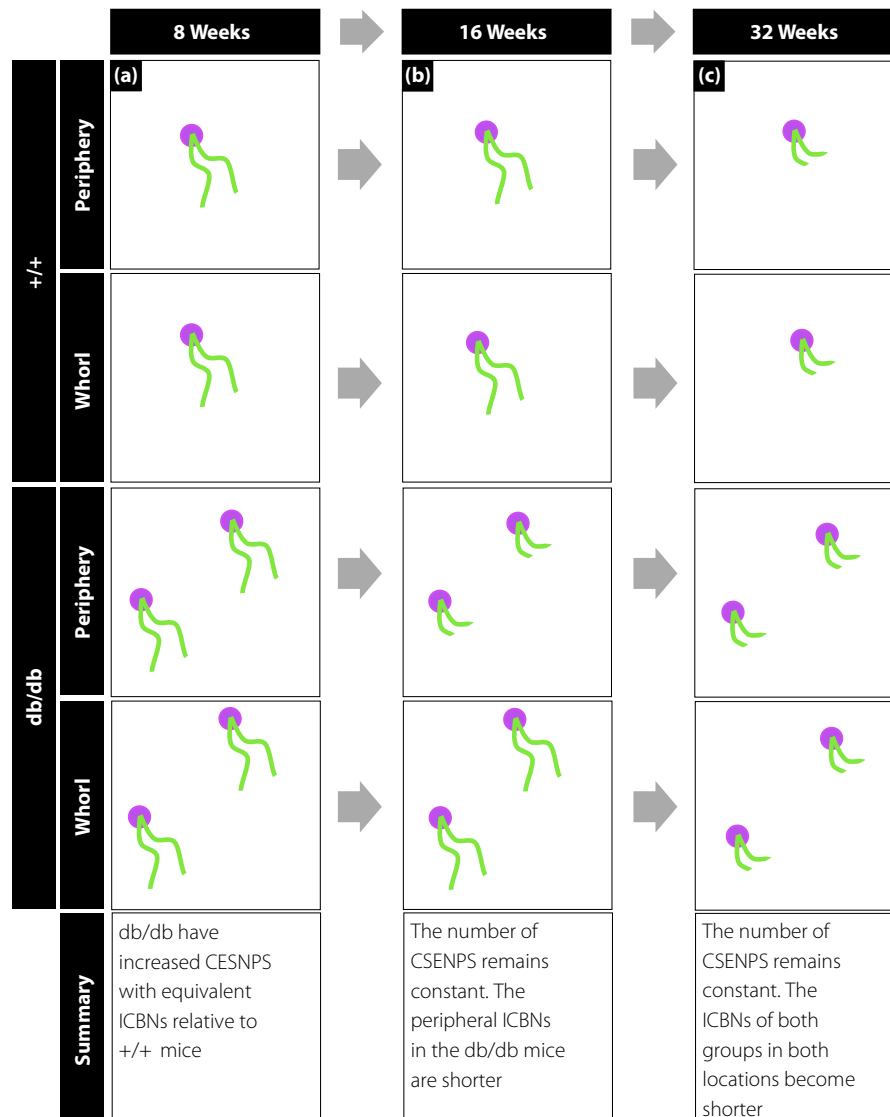


Figure 5 | Longitudinal changes undergone by CSENPS and ICBNs in type 2 diabetes. Diagrammatic representation of CSENPS (lilac circles) and ICBNs (green lines) from +/+ controls and *db/db* mice in the periphery and at the whorl are illustrated at sequential time points. At 8 weeks (a), ICBNs exiting each CSENPS were of relatively equal length, however, the number of CSENPS in *db/db* mice was increased. At 16 weeks (b), ICBNs in *db/db* mice became shorter in the periphery whilst those at the whorl were unaffected. At 32 weeks (c), the ICBNs exiting all CSENPS become truncated in both the center and the periphery, in both groups.

fed mice (26%) (compared with their respective controls; Figures 2a and 4a). While we did not measure insulin concentrations, prior research has demonstrated greater elevations in *db/db* mice relative to those fed a HFD¹¹, suggesting a possible association between these two values.

With disease progression, plasma insulin concentrations decline, and the products of the metabolic derangement induced by hyperglycemia predominate^{26,27}. The shift in this balance could explain the changes seen in ICBNs at 16 weeks in *db/db* mice²⁵ (Figures 1 and 5b). Following the initial neuronal expansion, ICBNs regressed to levels displayed in +/+

mice. However, this occurred without a change to the number of CSENPS, which remained significantly elevated (Figure 2a). Correspondingly, a decrease in the length of ICBNs exiting each CSENPS was detected, reaching significance in the periphery (Figures 2c and 5b). There are several possible pathophysiological explanations for such dynamic shifts in innervation. One is that this is a length-dependent neuropathy, i.e., the most distal aspects of nerves, being the ICBNs, are damaged first, before any impact on their penetration sites. However, it could also indicate that the insult targets ICBNs which are more vulnerable, whilst stromal axons and CSENPS are spared.

At 32 weeks, *db/db* and control mice exhibited reductions across all nerve parameters, yet the CSENPS remained constant (Figures 1, 2a, 5c). This suggests the ICBN degeneration was most likely an age-related effect^{9,28}. Notably, the number of CSENPS in *db/db* mice remained significantly elevated, and in both groups, penetration sites remained relatively constant over the monitoring period.

Another parameter used to monitor corneal nerves was their alignment⁹. This parameter evaluates the relationship between the direction of adjacent ICBN fibers instead of the curvature of individual axons. It functions as a composite measure of the guidance factors that influence the movement of ICBNs within the local microenvironment; with scores approaching zero indicating a deviation from the standard architecture. At all the time points monitored, *db/db* mice demonstrated no change in corneal nerve alignment compared with *+/+* (Figure 1p,t), signifying that the early axonal growth was unlikely to be a pathological reaction, rather an excessive physiological response⁹. In contrast, mice fed a HFD experienced an increase in axon alignment in the peripheral cornea (Figure 3h). Given the ICBNs did not elongate (rather their length was likely reduced) (Figures 3e,i and 4c,d), the increase computed may represent an artifact where the lower nerve density reduces the number of ICBNs capable of being 'out of alignment' thereby inflating the value of this parameter.

The dynamics with which CSENPS and ICBNs are modulated have important implications for how DPN progression is detected and monitored, but also for understanding the underlying pathophysiology of this disease process. In terms of detection, the most significant and rather surprising finding was that the initial phase of type 2 diabetes was heralded by an increase rather than a decrease in innervation (Figures 1 and 2). In humans, this expansion is likely to be subtle, but with further improvements in IVCM and software for image analysis, it could become a critically relevant phase that clinicians utilize. Furthermore, if imaging CSENPS becomes routine in clinical practice, this could become another valuable parameter that increases the sensitivity and specificity of screening investigations. Given their homogenous distribution (Figure S2b), imaging representative regions of the cornea should be sufficient, as has been demonstrated for the quantification of ICBNs²⁹. Finally, we provide evidence to suggest that the peripheral cornea is more sensitive to changes in ICBN parameters in terms of growth and regression in a diabetic paradigm. Consequently, it may be the best region for image acquisition to detect the earliest changes associated with type 2 diabetes.

From a pathophysiological standpoint, this study complements and extends prior investigations, especially regarding the location where nerve degeneration occurs. As a peripheral neuropathy, it has been postulated that axons within the inferior whorl are damaged first, as it consists of the most distal ICBN fibers³⁰. Accordingly, studies have shown that the whorl provides a better measure of ICBN damage than nerve fibers at

the apex of the cornea^{30,31}. This seemingly contradicts the data from our study, where neurodegeneration predominated at the periphery compared with the whorl. Importantly, it must be clarified that the whorl is a para-central structure and is thus relatively peripheral to the corneal apex. We hypothesize that soluble factors in blood regulate this phenomenon. Despite the cornea being an avascular tissue, it has a prominent vascular plexus in its periphery, allowing blood products to diffuse towards the center³². Accordingly, neurotoxic metabolites from blood accumulate at higher concentrations in the periphery compared with central regions. Additional evidence supporting this supposition was found when we examined tile scans of the entire cornea, where ICBNs originating in the peripheral cornea did not extend across to the whorl (Figure S2a,b). Rather, the ICBNs which formed the whorl originated from CSENPS much closer to the center. As such, ICBNs in the center are not substantially more 'distal' than those in the periphery but are likely spared from the damaging metabolic by-products of type 2 diabetes. Interestingly, the converse appears to be true for the CSENPS, whereby there was no spatial preference for their location, indicating that the growth signal for these sites likely arose from a central source.

We acknowledge that our study has several limitations. The first being that only a portion of the ICBNs was analyzed per cornea. Given the curvature of the cornea, it is not possible to image at a consistent depth and to capture exclusively the ICBNs⁹. Accordingly, a compromise in image size was required, which may have resulted in under sampling. Another limitation to consider is the high correlation between many of the currently used parameters. For example, length and density are highly related, and as such, once ICBN length has been accounted for, density adds little additional information. Additionally, alignment appears to be impacted by the density of ICBNs present, demonstrating it will require further refinement to expand its applicability in other diseases. These issues exemplify the importance of identifying and developing new metrics, such as the number of CSENPS, which are completely independent of other parameters and thus provide additional information that will increase the diagnostic capabilities of corneal IVCM.

FUNDING

This work was supported by a Diabetes Australia and an Australian National Health and Medical Research Council (1101078) research grant to N.D. as the PI. N.J.S. was supported by a National Heart Foundation of Australia Future Leader Fellowship (101153) and M.A.M. by an Australian Government Research Training Program Scholarship.

DISCLOSURE

The authors declare no conflict of interest.

Approval of the research protocol: All animal procedures were approved by the UNSW Animal Research Ethics Committee (18/102B and 18/131A). All investigations on mice were

conducted in accordance with the Australian Code of Practice for the Care and Use of Animals for Scientific Purposes.

Informed consent: N/A.

Registry and the registration no. of the study/trial: N/A.

Animal studies: All animal experiments were conducted following the national guidelines and the relevant national laws on the protection of animals.

REFERENCES

- Hicks CW, Selvin E. Epidemiology of peripheral neuropathy and lower extremity disease in diabetes. *Curr Diab Rep* 2019; 19: 86.
- Azmi S, Petropoulos IN, Ferdousi M, *et al.* An update on the diagnosis and treatment of diabetic somatic and autonomic neuropathy. *F1000Research* 2019; 8(F1000 Faculty Rev): 186.
- Malik RA, Kallinikos P, Abbott CA, *et al.* Corneal confocal microscopy: a non-invasive surrogate of nerve fibre damage and repair in diabetic patients. *Diabetologia* 2003; 46: 683–688.
- Oliveira-Soto L, Efron N. Morphology of corneal nerves using confocal microscopy. *Cornea* 2001; 20: 374–384.
- Ahmed A, Bril V, Orszag A, *et al.* Detection of diabetic sensorimotor polyneuropathy by corneal confocal microscopy in type 1 diabetes: a concurrent validity study. *Diabetes Care* 2012; 35: 821–828.
- Roszkowska AM, Licitra C, Tumminello G, *et al.* Corneal nerves in diabetes—the role of the in vivo corneal confocal microscopy of the subbasal nerve plexus in the assessment of peripheral small fiber neuropathy. *Surv Ophthalmol* 2021; 66: 493–513.
- Petropoulos IN, Ponirakis G, Khan A, *et al.* Corneal confocal microscopy: ready for prime time. *Clin Exp Optom* 2020; 103: 265–277.
- Kowtharapu BS, Winter K, Marfurt C, *et al.* Comparative quantitative assessment of the human corneal sub-basal nerve plexus by in vivo confocal microscopy and histological staining. *Eye (Lond)* 2017; 31: 481–490.
- Tuck H, Park M, Carnell M, *et al.* Neuronal-epithelial cell alignment: a determinant of health and disease status of the cornea. *Ocul Surf* 2021; 21: 257–270.
- Mouat MA, Wilkins BP, Ding E, *et al.* Metabolic profiling of mice with deletion of the orphan G protein-coupled receptor, GPR37L1. *Cell* 2022; 11: 1814.
- Burke SJ, Batdorf HM, Burk DH, *et al.* db/db mice exhibit features of human type 2 diabetes that are not present in weight-matched C57BL/6J mice fed a Western diet. *J Diabetes Res* 2017; 2017: 8503754.
- Marfurt CF, Cox J, Deek S, *et al.* Anatomy of the human corneal innervation. *Exp Eye Res* 2010; 90: 478–492.
- Patel DV, McGhee CN. Mapping of the normal human corneal sub-basal nerve plexus by in vivo laser scanning confocal microscopy. *Invest Ophthalmol Vis Sci* 2005; 46: 4485–4488.
- Obrosova IG, Ilnytska O, Lyzogubov W, *et al.* High-fat diet induced neuropathy of pre-diabetes and obesity: effects of “healthy” diet and aldose reductase inhibition. *Diabetes* 2007; 56: 2598–2608.
- Kneer K, Green MB, Meyer J, *et al.* High fat diet induces pre-type 2 diabetes with regional changes in corneal sensory nerves and altered P2X7 expression and localization. *Exp Eye Res* 2018; 175: 44–55.
- Alamri AS, Brock JA, Herath CB, *et al.* The effects of diabetes and high-fat diet on polymodal nociceptor and cold thermoreceptor nerve terminal endings in the corneal epithelium. *Invest Ophthalmol Vis Sci* 2019; 60: 209–217.
- Yorek MS, Obrosova A, Shevalye H, *et al.* Effect of diet-induced obesity or type 1 or type 2 diabetes on corneal nerves and peripheral neuropathy in C57Bl/6J mice. *J Peripher Nerv Syst* 2015; 20: 24–31.
- Quattrini C, Tavakoli M, Jeziorska M, *et al.* Surrogate markers of small fiber damage in human diabetic neuropathy. *Diabetes* 2007; 56: 2148–2154.
- Coppey LJ, Shevalye H, Obrosova A, *et al.* Determination of peripheral neuropathy in high-fat diet fed low-dose streptozotocin-treated female C57Bl/6J mice and Sprague-Dawley rats. *J Diabetes Investig* 2018; 9: 1033–1040.
- Coppey L, Davidson E, Shevalye H, *et al.* Progressive loss of corneal nerve fibers and sensitivity in rats modeling obesity and type 2 diabetes is reversible with omega-3 fatty acid intervention: supporting cornea analyses as a marker for peripheral neuropathy and treatment. *Diabetes Metab Syndr Obes* 2020; 13: 1367–1384.
- Duraikannu A, Krishnan A, Chandrasekhar A, *et al.* Beyond trophic factors: exploiting the intrinsic regenerative properties of adult neurons. *Front Cell Neurosci* 2019; 13: 128.
- Mahelkova G, Burdova MC, Mala S, *et al.* Higher Total insulin dose has positive effect on corneal nerve fibers in DM1 patients. *Invest Ophthalmol Vis Sci* 2018; 59: 3800–3807.
- Yorek MS, Obrosova A, Shevalye H, *et al.* Effect of glycemic control on corneal nerves and peripheral neuropathy in streptozotocin-induced diabetic C57Bl/6J mice. *J Peripher Nerv Syst* 2014; 19: 205–217.
- Weir GC, Bonner-Weir S. Five stages of evolving beta-cell dysfunction during progression to diabetes. *Diabetes* 2004; 53(Suppl 3): S16–S21.
- Arakawa K, Ishihara T, Oku A, *et al.* Improved diabetic syndrome in C57BL/KsJ-db/db mice by oral administration of the Na(+)-glucose cotransporter inhibitor T-1095. *Br J Pharmacol* 2001; 132: 578–586.
- Cashman CR, Hoke A. Mechanisms of distal axonal degeneration in peripheral neuropathies. *Neurosci Lett* 2015; 596: 33–50.
- Yagihashi S, Mizukami H, Sugimoto K. Mechanism of diabetic neuropathy: where are we now and where to go? *J Diabetes Investig* 2011; 2: 18–32.

28. Zhao K, Yu H, Zheng X, *et al.* Use of the inferior whorl for detecting age-related changes in human corneal subbasal nerve plexus with laser scanning confocal microscopy. *Ophthalmic Res* 2021; 64: 769–774.
29. Vagenas D, Pritchard N, Edwards K, *et al.* Optimal image sample size for corneal nerve morphometry. *Optom Vis Sci* 2012; 89: 812–817.
30. Kalteniece A, Ferdousi M, Petropoulos I, *et al.* Greater corneal nerve loss at the inferior whorl is related to the presence of diabetic neuropathy and painful diabetic neuropathy. *Sci Rep* 2018; 8: 3283.
31. Petropoulos IN, Ferdousi M, Marshall A, *et al.* The inferior whorl for detecting diabetic peripheral neuropathy using corneal confocal microscopy. *Invest Ophthalmol Vis Sci* 2015; 56: 2498–2504.
32. DelMonte DW, Kim T. Anatomy and physiology of the cornea. *J Cataract Refract Surg* 2011; 37: 588–598.

SUPPORTING INFORMATION

Additional supporting information may be found online in the Supporting Information section at the end of the article.

Appendix S1 | Supplementary Methods.

Table S1 | Composition of the high-fat diet.

Figure S1 | Acquisition of murine corneal nerve images.

Figure S2 | Identification and distribution of corneal stromal-epithelial nerve penetration sites.

Figure S3 | Blood glucose measurements.